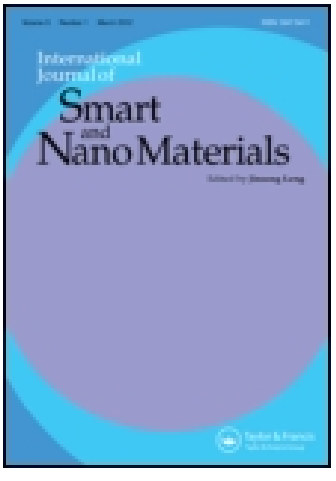

International Journal of Smart and Nano Materials

Publication details, including instructions for authors and subscription information:
http://www.tandfonline.com/loi/tsnm20

XRD study of intercalation in statically annealed composites of ethylene copolymers and organically modified montmorillonites. 2. One-tailed organoclays

Sara Filippi[a] & Giovanni Polacco[a]

[a] Department of Civil and Industrial Engineering, University of Pisa, Largo Lucio Lazzarino, 1, 56126 Pisa, Italy

Published online: 01 Apr 2014.

To cite this article: Sara Filippi & Giovanni Polacco (2014) XRD study of intercalation in statically annealed composites of ethylene copolymers and organically modified montmorillonites. 2. One-tailed organoclays, International Journal of Smart and Nano Materials, 5:1, 59-74, DOI: 10.1080/19475411.2014.902869

To link to this article: http://dx.doi.org/10.1080/19475411.2014.902869

International Journal of Smart and Nano Materials, 2014
Vol. 5, No. 1, 59–74, http://dx.doi.org/10.1080/19475411.2014.902869

Taylor & Francis
Taylor & Francis Group

XRD study of intercalation in statically annealed composites of ethylene copolymers and organically modified montmorillonites. 2. One-tailed organoclays

Sara Filippi* and Giovanni Polacco

Department of Civil and Industrial Engineering, University of Pisa, Largo Lucio Lazzarino, 1, 56126 Pisa, Italy

(*Received 8 November 2013; final version received 5 March 2014*)

Ethylene copolymers with different polar comonomers, such as vinyl acetate, methyl acrylate, glycidyl methacrylate, and maleic anhydride, were used for the preparation of polymer/clay nanocomposites by statically annealing their mechanical mixtures with different commercial or home-made organically modified montmorillonites containing only one long alkyl tail. The nanostructure of the products was monitored by X-ray diffraction, and the dispersion of the silicate particles within the polymer matrix was qualitatively evaluated through microscopic analyses. The effect of the preparation conditions on the structure and the morphology of the composites was also addressed through the characterization of selected samples with similar composition prepared by melt compounding. In agreement with the findings reported in a previous paper for the composites filled with two-tailed organoclays, intercalation of the copolymer chains within the tighter galleries of the one-tailed clays occurs easily, independent of the application of a mechanical stress. However, the shear-driven break-up of the intercalated clay particles into smaller platelets (exfoliation) seems more hindered. A collapse of the organoclay interlayer spacing was only observed clearly for a commercial one-tailed organoclay – Cloisite® 30B – whereas the same effect was almost negligible for a home-made organoclay with similar structure.

Keywords: ethylene copolymers; one-tailed organoclays; annealing; X-ray diffraction

1. Introduction

The stability of polymer/clay nanocomposites (PCNs) depends on the characteristics of polymer, silicate platelets, and organic clay modifier [1]. From the thermodynamic point of view, the equilibrium structures (intercalated/exfoliated) achievable when blending a polymer/organoclay couple can be reliably forecast [1]. In contrast, the kinetics and the mechanism of intercalation of the surfactant or polymer into the clay stacks are less understood even if studied since long time ago [2]. The intercalation process is influenced by the transport of polymer into the primary particles of the silicate [3], as well as by the degree of polymerization and of the length of the surfactant tails and/or the presence of functional groups along the macromolecules [4]. An important aspect is that the mobility of the polymer chains in the organoclay galleries is comparable to that in the bulk polymer melt. Therefore, PCN forms rapidly if the temperature is sufficiently higher than the glass

*Corresponding author. Email: s.filippi@diccism.unipi.it

transition, the average molecular weight is moderate, and the coverage of the silicate surface by organic surfactants is appropriate. This is confirmed by the fact that intercalation may be obtained also under static conditions [5–8].

Ethylene copolymers have been extensively employed in the preparation of PCNs, and reviews dedicated to polyolefin-based PCNs are available in the scientific literature [9–14]. The level of silicate layers dispersion in PCNs based on ethylene copolymers depends on the type, the concentration and the location of the functional groups on the polymer chains, the structure of the surfactant used for clay modification, the organoclay loading, etc. Usually, the composites prepared by solution blending contain unintercalated clay tactoids that underwent fast intercalation upon thermal treatment carried out at temperatures higher than the polymer melting point [15,16]. Recent studies suggested that organoclays with two long alkyl tails undergo better dispersion than those with a single tail [17–19]. However, opposite results were also described by other researchers [20–22]. Martins *et al.* suggested that these conflicting reports are possibly due to the different processing conditions [23]. This point is discussed in detail in this paper. In the previous paper of this series, the intercalation in statically annealed dry blends of different functionalized polyethylenes with organoclays modified with ammonium ion surfactants containing two long alkyl groups was investigated [24]. The structure and the morphology of the PCNs prepared by this procedure were compared with those of analogous materials produced with different methods, such as melt compounding and solution blending. The intercalation of the copolymer chains within the galleries of the organoclays occurs rapidly, independent of the application of shear stress. On the other hand, solution blending, proved unable, in the absence of subsequent thermal treatments, to yield intercalation. Moreover, the preliminary dispersion of micron-sized clay particles achievable by solution blending leads to even faster intercalation when the mixture is melted. For most of the polymer/organoclay couples studied in part 1 of this work [24], mixed intercalated/exfoliated structures were thermodynamically stable. However, the highest levels of exfoliation were obtained for the melt compounded PCNs prepared from polymer/clay couples with optimal match of polar characteristics.

In this work, the above study was extended to analogous composites loaded with modified montmorillonites (MMTs) organically modified with surfactants containing only one long alkyl tail, and the effect of a lowered interlayer distance and a higher polarity of the inorganic filler was investigated.

Commercially available organoclays differ for the structure of the organic modifier, the lateral dimensions, the charge density, and the cation exchange capacity (CEC). The latter plays an important role in the process of polymer chains intercalation. For this reason, most of the organoclays used in this work were prepared by modification of only one commercial Na-MMT (Dellite® LVF, with a CEC of 1.05 meq/g). The effect of a difference in the CEC values was also addressed using a couple of organoclays based on Cloisite-Na^+ (with a CEC of 0.926 meq/g), that is, the commercially available Cloisite® 30B and the home-synthesized C-ArqHT.

The ethylene copolymers used for the PCNs preparation were the same already used in the previous work [24]. Except for HDMA, which is a linear HDPE grafted with maleic anhydride (MA), all the other materials possess the branched structure typical for LDPE. HDMA is certainly the less polar copolymer, as the MA content is only 1 wt%. On the other hand, the presence of MA and glycidyl methacrylate (GMA) groups in the chains does probably enhance the interaction of these copolymers with the hydroxyl groups of the silicate layers.

2. Experimental part

2.1. Materials

The organoclays used in this work are indicated in Table 1, with their sources, the CEC, the milliequivalent exchange ratio (MER), the loss on ignition, and the d_{001} spacing determined by XRD. The surfactants used for MMT modification are the quaternary ammonium chlorides indicated by symbols, where H is hydrogen, C18 is *n*-octadecyl, M is methyl, T is 'tallow', that is, a partly unsaturated alkyl chain with approximate composition: 65% C18; 30% C16; 5% C14, (HT) is 'hydrogenated tallow', (HE) is 2-hydroxyethyl, and O is oleyl.

Cloisite® 30B (from Southern Clay Products Inc., USA), and C-ArqHT were prepared from Cloisite-Na^+, having a CEC of 0.926 meq/g. D-ODA, D-ArqHT, and D-Eth were synthesized from Dellite® LVF (CEC = 1.05 meq/g; Laviosa Chimica Mineraria S.p.A., Italy) by cation exchange with, respectively, octadecyl ammonium (ODA) chloride and the commercial $M_3(HT)_1$ and $M_1(HE)_2O$ surfactants (Arquad HT-50 and Ethoquad O/12, by Akzo Nobel).

The polymers used as matrixes are listed in Table 2, together with their sources and some of their characteristics. EVA14, EVA28, EMA, EGMA, and EAGMA are random

Table 1. Organoclays[a].

Clay code	Commercial designation	Surfactant[b]	CEC[c] (meq/g)	MER[d] (meq/g)	Loss on ignition (wt%)	d_{001}[e] (nm)
D-ODA	Experimental	H_3C_{18}	1.05	1.05[f]	28	2.03
D-ArqHT	Experimental	$M_3(HT)_1$	1.05	1.05[f]	29	2.22
D-Eth	Experimental	$M(HE)_2O$	1.05	1.05[f]	29	2.06
30B	Cloisite® 30B	$M(HE)_2T$	0.926	0.90	30	1.85
C-ArqHT	Experimental	$M_3(HT)_1$	0.926	0.926[f]	27	1.92

Notes: [a]The data for Cloisite® 30B, produced by Southern Clay Products Inc., are from the supplier's product bulletin. [b]cf. 'Experimental' for an explanation of the symbols. [c]Cation exchange capacity. [d]Milliequivalent exchange ratio (modifier used per g of native clay). [e]Interlayer spacing. [f]cf. 'Experimental'.

Table 2. Ethylene copolymers (supplier's data).

Sample code	Functional comonomer(s) (wt%)	Commercial designation (supplier)	Structure	MFI (dg/min)	Density (kg/m^3)	T_m (°C)
EVA14	VA[a] 14	Greenflex® FC45 (Polimeri Europa)	E-*ran*-VA	0.3	—	93
EVA28	VA 28	Greenflex® HN70 (Polimeri Europa)	E-*ran*-VA	6	—	73
EMA	MeA[b] 20	Elvaloy® 1820AC (DuPont)	E-*ran*-MeA	8	942	92
EGMA	GMA[c] 8	Lotader® AX8840 (Arkema)	E-*ran*-GMA	5	940	109
EAGMA	GMA – MeA 3–24	Lotader® AX8930 (Arkema)	E-*ran*-GMA-*ran*-MeA	6	940	66
HDMA	MA[d] 1	Polybond® 3009 (Chemtura)	HDPE-*g*-MA	3–6	950	127

Notes: [a]Vinyl acetate. [b]Methyl acrylate. [c]Glycidyl methacrylate. [d]Maleic anhydride.

copolymers with branched structure. The polymers were dried in a vacuum oven at 65°C for 2 days before use.

2.2. Procedures

D-ODA, D-ArqHT, D-Eth, and C-ArqHT were synthesized as follows: 15 g of Dellite® LVF (or Cloisite-Na) were stirred for 2 h in 1000 mL of deionized water at 80°C; 200 mL of a water solution of the appropriate surfactant (20% excess, with respect to stoichiometry) was added, and the mixture was mechanically stirred for 24 h at 80°C. The precipitate was collected on a sintered glass filter, washed with warm water and, successively, with EtOH in order to remove the excess surfactant. Thus, the MER of organoclays is nominally indicated in Table 1 as equal to the CEC of the starting MMT. The organoclays were dried in a vacuum oven at 40°C for 24 h, milled in a mortar and sieved (200 mesh).

The statically annealed (s.a.) composites were prepared as follows: mechanical blending the polymers and the clays, as powders of micrometric dimensions; shaping the mixtures into tablets of 20 mm diameter and 2 mm thickness in a Carver press; heating the tablets at temperatures slightly higher than the polymer melting point for about 10 min; slow cooling to room temperature.

The melt compounded (m.c.) composites were prepared in a Brabender Plasticorder mixer of 50 mL capacity, preheated to 120°C (for EVA14, EVA28, EMA, EGMA, and EAGMA) or 150°C (for HDMA). The rotor speed was maintained at 30 rpm for about 3 min after addition of the polymer/clay mixtures, and was then increased gradually (in 30 s) to 60 rpm. During the kneading time (10 min), the temperature increased by 10–15 K due to stress heating. The molten composites were extracted from the mixer and cooled naturally in air.

The loss on ignition of the experimental organoclays was determined by thermogravimetric analysis with a Q500 TA Instruments balance using a sample of about 10 mg. The test was made in air (60 mL/min), in the 30–900°C temperature range, with a scanning rate of 10°C/min.

X-ray diffraction measurements (CuK_α) were made in reflection mode with a Siemens D500 Krystalloflex 810 apparatus at a scan rate of 1.0° min^{-1}. The clay was analyzed as a powder, whereas the composites were in the form of disks of 20 mm diameter and 2 mm thickness.

Polarized optical microscopy (POM) observations were made at 150°C on a Leitz Ortholux microscope equipped with a Linkam TMS 93 hot stage and a digital camera JVC TK-1085E. A small fragment of the composite samples was placed on a glass slide, heated at 150°C, and pressed with a cover slip to obtain a film of 80–100 μm thickness. Observations were made under crossed polarizers, whereby the micron-sized clay agglomerates, if any, were easily revealed as highly birefringent particles.

3. Results and discussion

The XRD patterns of D-ODA and those of its 5 wt% m.c. and s.a. composites with EVA14, EVA28, and EMA are reported in Figure 1. Figure 2 shows similar patterns for the composites with HDMA, EGMA, and EAGMA.

The first-sight conclusion one can draw from the two figures is that there is a qualitative similarity between the structures of the corresponding m.c. and s.a. composites. In fact, the position of the low-angle peaks on the 2θ scale is independent of the

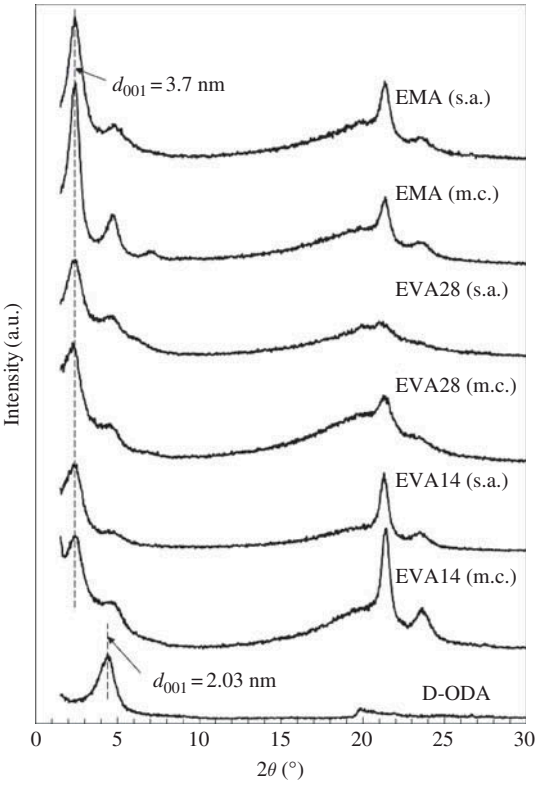

Figure 1. XRD patterns of D-ODA and its 5 wt% m.c. and s.a. composites with EVA14, EVA28, and EMA.

preparation protocol. This means that the shear stress acting on the polymer/clay mixtures during the melt compounding has little influence, if any, on nanostructure formation.

All the composites of Figure 1 display an intense reflection at $2\theta \approx 2.38°$, with higher orders at 4.75° and 7.1°, corresponding to a regular d_{001} spacing of 3.7 nm, in fair agreement with the results found by Tian *et al.* [25] for an EVA/organoclay nanocomposite. This demonstrates that the D-ODA was intercalated by the EVA and EMA chains, and the penetration of the copolymer chains caused a considerable increase of the 2.03 nm interlayer distance of the organoclay. Moreover, the similarity of the XRD profiles of the m.c. and s.a. samples suggests that the resulting structure is thermodynamically stable for these systems. It should be pointed out that melt compounding EVA with an ODA-modified MMT was found by Zanetti *et al.* [26] to cause a shift to wider angles of the basal reflection of the nanofiller. This effect, attributed by the authors to the possible presence of unmodified MMT left in the organoclay, or to partial degradation of the latter [26], was apparently absent in our system as well as in that of Tian *et al.* [25].

The behavior of the composites shown in Figure 2 is somehow different. Let us deal with the EGMA and EAGMA composites, first. Here also, intercalation occurred, independent of the application of a shear stress during the preparation. However, the extent of gallery height expansion was slightly larger than that observed for the EVA and EMA composites. The capability of the GMA groups of the copolymers to efficiently interact with the silicate layer surface may probably explain this difference. It can also be observed that,

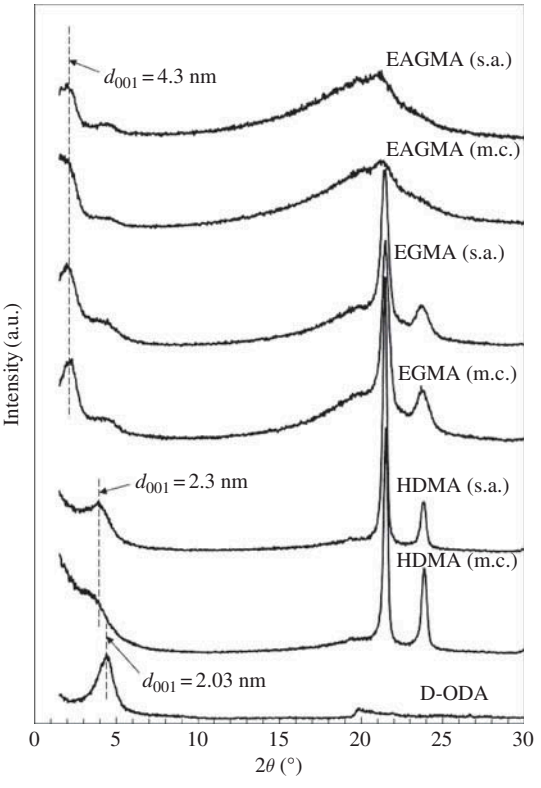

Figure 2. XRD patterns of D-ODA and its 5 wt% m.c. and s.a. composites with HDMA, EGMA, and EAGMA.

especially for the composite based on the more polar EAGMA, and notably for the m.c. sample, the basal reflection is very weak and broad and is accompanied by a continuous increase of reflected intensity at low angles, thus suggesting a level of clay exfoliation.

Finally, in the XRD patterns of the D-ODA composites based on EGMA and EAGMA, the weaker peak seen at 2θ angles of 4.35° probably comprise a contribution of unintercalated organoclay stacks rather than being just the second order of the basal reflection, which should otherwise appear at $2\theta \approx 4.1°$. By the way, a second-order peak would not be expected to be visible in these XRD patterns, given the low intensity and broadness of the basal reflections. Thus, for these copolymer/clay mixtures, the intercalation process is not so fast so that a small amount of unintercalated stacks is still present at the end of the sample preparation. However, despite the slower penetration of the copolymer chains within the D-ODA galleries, once intercalation has occurred, it tends to proceed further, particularly in the melt kneaded composite, toward exfoliation (notice that the basal reflection did almost fade in the m.c. sample).

The XRD patterns of the HDMA/D-ODA composites shown in Figure 2 suggest that the behavior of these materials differs even more from that of the systems of Figure 1. As already pointed out, HDMA comprises predominantly linear chains with a very limited number of grafted succinic anhydride groups. The overall polarity of these polymers is rather low, but the anhydride functionalities can probably lead to hydrogen bonding with the silicate layers. As shown in Figure 2, intercalation of the HDMA chains within the

D-ODA galleries seems to take place rapidly, though leading to a modest expansion of the interlayer space. However, a comparison of the diffractograms of the s.a. and m.c. samples suggests that the mechanical stress acting on the system during melt compounding helps disrupt progressively the intercalated stacks so that the level of exfoliation increases. Actually, the XRD profile of the m.c. sample retains just a broad shoulder at $2\theta \approx 3.8°$, ascribable to intercalation, on a background of continuously increasing reflected intensity pointing to exfoliation. This conclusion is also supported by the finding that the I_{110}/I_{200} intensity ratio of the reflections at $2\theta \approx 21.6°$ and 24.0° of the crystalline structure of HDMA is considerably lower for the m.c. sample (~2.5 vs. ~4 for the s.a. composite). As it was shown elsewhere [16], an intensity ratio lower than ~3 is indicative of a preferred orientation of both polymer crystallites and silicate platelets parallel to the specimen surface and the effect is particularly evident for highly exfoliated, m.c., and compression molded PCNs. Thus, the XRD patterns of the HDMA/D-ODA nanocomposites shown in Figure 2 suggest that the intercalated clay stacks, formed upon melting the polymer/clay mixture, slowly decompose into smaller particles (exfoliation [27]), and the process is favored by mechanical treatment.

The behavior of the composites loaded with D-ArqHT was found to resemble that discussed before for the analogous materials containing the D-ODA clay. For the sake of brevity, only the XRD traces recorded for the s.a. composites based on EVA14, EVA28, EMA, EGMA, and EAGMA are given in Figure 3. The XRD patterns of the analogous

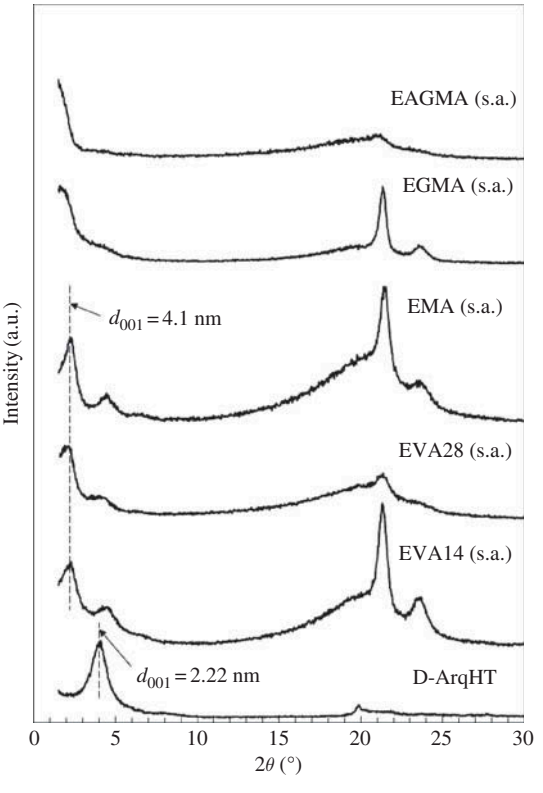

Figure 3. XRD patterns of D-ArqHT and its 5 wt% s.a. composites with EVA14, EVA28 and EMA, EGMA, and EAGMA.

m.c. materials (not shown) were very similar. Thus, the conclusions drawn before with reference to the effect played on intercalation by the stress acting on the system in the melt compounding preparations are also valid for the present PCNs.

The substitution of the three hydrogen atoms of the D-ODA modifier with three methyl groups leads to an increase of the organoclay spacing to d_{001} = 2.22 nm. The interlayer distance measured by XRD for the intercalated EVA and EMA nanocomposites filled with D-ArqHT is slightly larger than that of the analogous nanocomposites loaded with the D-ODA clay, shown in Figure 1 (4.1 vs. 3.7 nm).

The increased hydrophobicity of D-ArqHT compared with that of D-ODA has probably improved the affinity of the organoclay toward the EGMA and EAGMA copolymers. The XRD patterns of the composites based on the latter copolymers are almost free of the low-angle reflections of regularly stacked silicate layers, thus suggesting that the interaction of the D-ArqHT organoclay with these molten copolymers (in particular, EAGMA) led to extensive decomposition of the large silicate booklets into smaller and/or disorganized particles.

In agreement with the results found by others for the EVA composites with similar clays [28,29], no clear indication of D-ArqHT degradation was found in this study.

The XRD profiles recorded for the m.c. and s.a. composites of all the copolymers with the D-Eth nanofiller are reported in Figures 4 and 5. Once more, the qualitative close

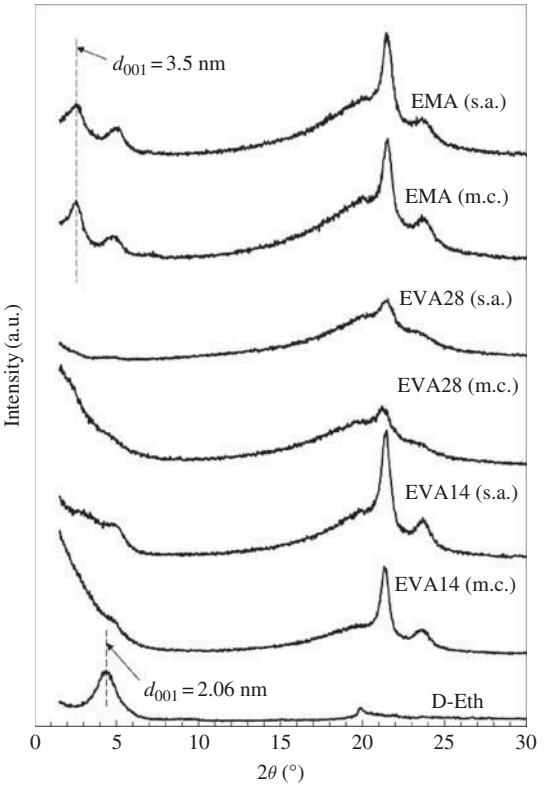

Figure 4. XRD patterns of D-Eth and its 5 wt% m.c. and s.a. composites with EVA14, EVA28, and EMA.

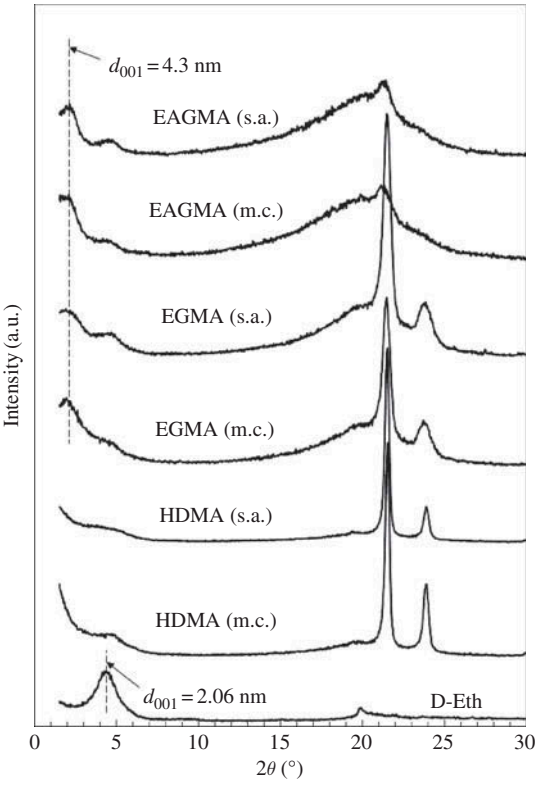

Figure 5. XRD patterns of D-Eth and its 5 wt% m.c. and s.a. composites with HDMA, EGMA, and EAGMA.

similarity between the structures of the m.c. and s.a. composites is confirmed for the majority of the materials considered in the figures.

The EVA composites, particularly that based on EVA28, display almost silent XRD patterns in the low-angle region. This indicates a high level of exfoliation and/or disordered intercalation. It should be remembered that the structure of the D-Eth organoclay is very similar to that of the commercial Cloisite® 30B (30B) that was extensively used for the preparation of EVA/organoclay nanocomposites [18,20–22,29–33]. The latter composites were also found to possess an appreciable level of exfoliation.

The XRD spectra of the EVA/D-Eth composites, especially that based on EVA14, comprise a weak reflection at wider angles compared with that of D-Eth ($2\theta \approx 5.0°$ vs. 4.33°), suggesting that a small amount of the organoclay may undergo a modest interlayer spacing collapse, similar to that often observed for the EVA/30B composites [18,29–33]. This point is discussed in more detail below.

The XRD patterns of the EMA/D-Eth composites shown in Figure 4 are typical for intercalated nanocomposites characterized by a d_{001} interlayer distance of 3.7 nm. Given that the functional groups of EMA and those of the EVA copolymers are isomeric and their contents are comparable, it may be surprising that the structures of the relevant nanocomposites are different. We cannot offer any definite explanation for this. Another apparent peculiarity of the EMA/D-Eth spectra is that the reflection at $2\theta \approx 5.0°$ is perhaps too intense to be ascribed to the second order of the basal reflection of the intercalated

clay stacks at $2\theta \approx 2.51°$. This peculiarity might be rationalized assuming that a collapse of the d-spacing of the D-Eth organoclay, such as that previously envisaged for the EVA composites, has also taken place during the preparation of the EMA composites. This would lead to a superposition of the two peaks. However, we do not avail of any clear evidence supporting this hypothesis.

The XRD patterns of the EGMA and EAGMA composites shown in Figure 5 comprise low-angle reflections ($2\theta \approx 2.05°$) ascribable to intercalation. In place of the second-order peaks that, if present, would be expected to appear at $2\theta \approx 4.1°$, broad reflections around $2\theta \approx 4.6°$ are seen in the spectra. Once more, the overlapping of the second-order reflection and a peak due to collapsed tactoids of the D-Eth clay might explain this observation. Although we have no direct proof in favor of such hypothesis, a circumstantial supporting evidence is provided by the XRD patterns of the HDMA/D-Eth composites shown in the same figure. Indeed, neither of the HDMA patterns displays reflections at 2θ angles lower than that of the organoclay, thus demonstrating the absence of regularly intercalated silicate booklets. Just a continuous increase of reflected intensity suggesting exfoliation, plus a reflection close to $2\theta \approx 5°$, is visible in these spectra. The latter reflection must therefore be ascribed to silicate layers stacks with decreased spacing. Thus, the hypotheses illustrated above, that a collapse of the D-Eth organoclay may have taken place during the preparation and processing of the other nanocomposites, too, may appear reasonable.

Collapse of the interlayer spacing of organically modified clays, more notably those containing one-tailed quaternary ammonium ions, was observed in many studies, and generally described as due to thermal degradation of the organic component, with expulsion of the degradation products. In particular, several nanocomposites produced by melt compounding from EVA [18,29–33] and other polymers [5,34–38], with 30B as nanofiller, were found to display XRD patterns comprising reflections at 2θ angles wider than that of the organoclay. Only in a few reports on the preparation and characterization of EVA/30B nanocomposites [20–22] a shift of the basal reflection toward wider angles was apparently not found.

In a recent investigation, Benali *et al.* [39] compared the behavior of 30B with that of other organoclays modified with surfactants containing hydrogenated alkyl tails in place of the partly unsaturated [40] 'tallow' (T) groups of the 30B. The authors concluded that the decrease of the d-spacing is probably due to oxidation and cross-linking of the unsaturated alkyl tails.

As shown in Figure 6, the m.c. EVA14/30B composite prepared by us does show a well-resolved reflection at $2\theta \approx 6°$, corresponding to a collapsed d-spacing of ~1.47 nm. The XRD patterns of 30B and its EVA14 composite are compared in Figure 6 with those, already discussed above, of D-Eth and the analogous EVA14 composite.

From Figure 6 we conclude that, even if the shoulder seen at $2\theta \approx 5°$ ($d_{001} \approx 1.77$ nm) in the XRD pattern of the EVA14/D-Eth is actually due to tactoids with collapsed interlayer spacing, the amount of such tightened tactoids is considerably lower than that in the analogous 30B composite. In this respect, it may be interesting to point out that D-Eth was prepared by cation exchange with a surfactant (Ethoquad O12, by Akzo Nobel) comprising oleyl groups. Therefore, most of the long tails of this organoclay contain a double bond, whereas the modifier employed to synthesize the 30B has only 50% of unsaturated alkyl groups [40]. Thus, unsaturation of the organic component cannot be the (only) parameter responsible for the behavior of 30B. On the other hand, this organoclay was found to undergo a d-spacing collapse even when processed at temperatures lower than that (~180°C) of the onset of thermal degradation. Moreover, the presence of excess

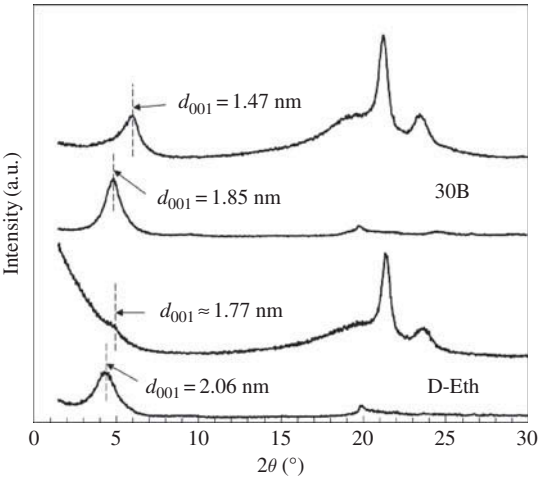

Figure 6. XRD patterns of D-Eth and 30B, together with their 5 wt% m.c. composites with EVA14.

surfactant (and/or other impurities) in the commercial product was shown to lower the thermal stability of this organoclay [41] and to enhance the phenomenon of gallery height shrinkage [42]. All this matter is being studied further in our laboratories, and the results will be published in a forthcoming paper.

In Figure 7, the effect of the organoclay CEC on the intercalation process is addressed. The two organoclays C-ArqHT and D-ArqHT differ from each other for the charge density of the starting MMT's: Cloisite Na^+ and Dellite® LVF (CEC = 0.926 vs. 1.05 meq/g). Due to the higher content of organic component, the interlayer spacing of D-ArqHT (2.22 nm) is larger than that of C-ArqHT (1.92 nm). As shown in the figure, however, intercalation of the EMA chains within the galleries of these organoclays leads, for both composites, to the same d-spacing of 4.1 nm.

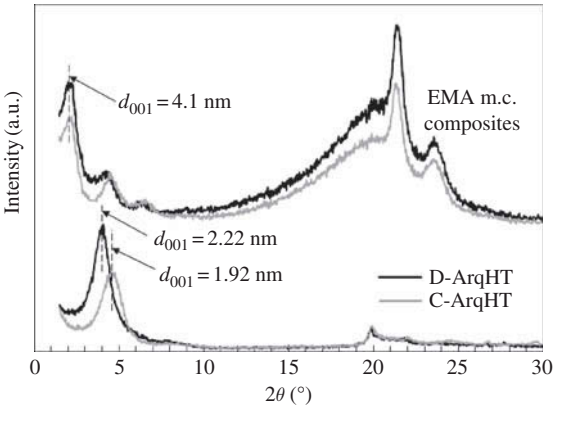

Figure 7. XRD patterns of C-ArqHT and D-ArqHT, and those of their 5 wt% m.c. composites with EMA.

The same behavior was already observed in the previous paper [24] for a couple of two-tailed clays with different CEC.

The Cloisite® 20A and D-ArqHC organoclays, modified with the same $M_2(HT)_2$ surfactant, displayed d-spacings of 2.42 and 3.05 nm, respectively, due to the different CEC of their precursor MMTs. However, the EVA14 PCNs loaded with the two clays possess an intercalated nanostructure with the same interlayer spacing of 3.91 nm (cf. Figures 1 and 2 of [24]).

The finding that CEC has almost no effect on the d-spacing of the intercalated nanocomposites prepared with different organoclays (modified with the same organic cations) may appear surprising, at first sight. However, this behavior can probably be rationalized considering that the thermodynamics of the intercalation process taking place in highly compatible polymer/organoclay mixtures depends on the equilibrium interlayer distance, that is, on the volume of organic material filling the galleries, rather than on the relative content of the two components of this material (ionically bonded clay modifier and polymer chains).

The morphology of the nanocomposites prepared from functionalized polyethylenes and one-tailed organoclays differs from that of the analogous composites loaded with two-tailed organoclays described in part 1 of this work [24]. For the latter PCNs, the morphology depends not only on the affinity between polymer and clay but also on the preparation method. Although intercalation occurs rapidly, independent of the application of mechanical stress, an excellent dispersion of submicrometric silicate particles within the polymer matrix was only observed when the molten polymer/clay mixture was kneaded in a mixer. The composites prepared by static annealing displayed morphologies characterized by the presence of poorly dispersed particles with dimensions of microns or even tens of microns. For the PCNs described in this paper, on the contrary, the effect of the preparation protocol seems to be less important, if any. In Figure 8, a few examples of the optical micrographs taken under crossed polarizers on molten films of some s.a. and m.c. composites are shown and compared with those of analogous m.c. samples loaded with a two-tailed organoclay (Cloisite® 20A).

The POM micrographs (a) and (e) of the EMA/D-Eth andEVA14/30B s.a. composites, respectively, demonstrate that the morphology of these materials is very similar to that of the analogous s.a. composites with two-tailed organoclays described before.

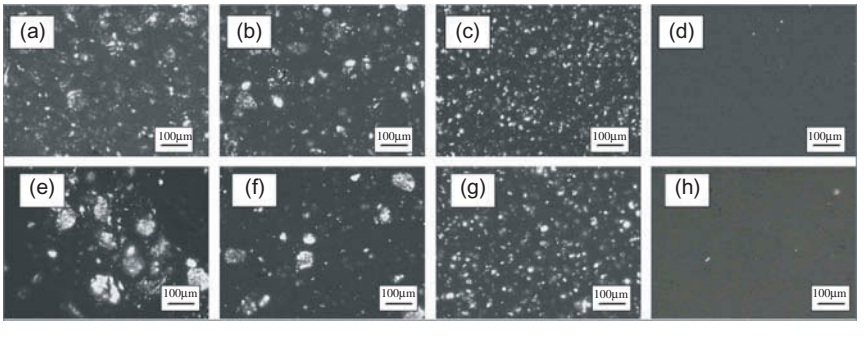

Figure 8. POM images of the EMA (above) and EVA14 (below) nanocomposites with 5 wt% of (a) D-Eth (s.a.); (b) D-Eth (m.c.); (c) 30B (m.c.); (d) Cloisite® 20A (m.c.); (e) 30B (s.a.); (f) D-Eth (m.c.); (g) 30B (m.c.); (h) Cloisite® 20A (m.c.).

In contrast, it was not expected that, as demonstrated by the micrographs (b), (c), (f), and (g), even after melt compounding, the micron-sized aggregates of the one-tailed organoclays failed to completely crumble into submicrometric particles as it was observed for the two-tailed organoclays (cf. the micrographs (d) and (h) in Figure 8). Results very similar to those illustrated in Figure 8 were also found from the morphological analysis carried out either by POM and by scanning electron microscopy on all the other polymer/clay couples described in this work.

It may be interesting to compare the POM micrographs (f) and (g) of Figure 8, taken on the m.c. composites EVA14/D-Eth and EVA14/30B, in the light of the XRD patterns of the same samples, shown in Figure 6. The second composite is known from the literature [18,20–22,29–33] to possess a high level of exfoliation. On the other hand, the XRD pattern displays a fairly intense reflection at $2\theta \approx 6°$ associated with unintercalated tactoids with collapsed d-spacing, and the bright micrometric particles seen in the POM image of this sample (Figure 8g) might be ascribed to their presence. Therefore, the EVA14/30B composite comprise a dispersed phase of unintercalated clay particles and a matrix, appearing as a black background in the micrograph, made up of a fine dispersion of exfoliated silicate platelets. The XRD pattern of the EVA14/D-Eth sample, on the contrary, shows just a hint of a reflection ascribable to collapsed tactoids and, consequently, the latter would be expected to eventually appear in the relevant POM image as very few and small bright spots. The micrograph of Figure 8f depicts a different situation: the black area is larger and the number of bright particles is lower, but the size of some of them is much larger. Considering that the small-angle region of the XRD spectrum of this sample displays a strong progressive increase of diffracted intensity, one might speculate that this is due to a population of silicate booklets or aggregates, characterized by an increasing level of intercalation and low packing regularity. At any rate, whatever is the true origin of the different behavior of 30B and the structurally similar D-Eth, it is no doubt the result of the different CEC. This point also needs further investigation.

4. Conclusions

The results of the present study indicate that the investigated ethylene copolymers do easily glide within the galleries of one-tailed organoclays, independent of the application of mechanical stress. The speed of the process, probably because of the smaller d-spacing, is a bit lower than with two-tailed clays. For both types of organoclays, the intercalated structures revealed by XRD are generally similar for the s.a. and m.c. composites, suggesting that they correspond to thermodynamic equilibrium. Exfoliation of the intercalated silicate booklets or aggregates, that is, their shear-driven decomposition into smaller platelets [27], is more difficult and slower for the MMTs modified with one-tailed surfactants. As a result, the morphology of the m.c. composites filled with the latter organoclays was characterized by the presence of many micron-sized, intercalated (according to XRD), silicate particles.

Probably due to the moderate temperatures employed in this work for the preparation and processing of the nanocomposites, the *d*-spacing collapse often reported for the clays with only one long alkyl group was shown to be remarkable only for the commercial 30B organoclay. For the structurally similar D-Eth clay, synthesized in our laboratory, the above effect was almost negligible despite the higher level of unsaturation of the alkyl tails.

References

[1] Q.H. Zeng, A.B. Yu, and G.Q. Lu, *Multiscale modeling and simulation of polymer nanocomposites*, Prog. Polym. Sci. 33 (2) (2008), pp. 191–269. doi:10.1016/j.progpolymsci.2007.09.002.

[2] S.A. Solin, *Kinetics and diffusion in graphite intercalation compounds*, in *Intercalation in Layered Materials*, Vol. 148, NATO ASI Ser. B, Phys., M.S. Dresselhaus, ed., Plenum Press, New York, 1986, pp. 173–183. doi:10.1007/978-1-4757-5556-5_14.

[3] R.A. Vaia, K.D. Jandt, E.J. Kramer, and E.P. Giannelis, *Kinetics of polymer melt intercalation*, Macromolecules 28 (24) (1995), pp. 8080–8085. doi:10.1021/ma00128a016.

[4] E. Manias, H. Chen, R. Krishnamoorti, J. Genzer, E.J. Kramer, and E.P. Giannelis, *Intercalation kinetics of long polymers in 2 nm confinements*, Macromolecules 33 (2000), pp. 7955–7966. doi:10.1021/ma0009552.

[5] J.T. Yoon, W.H. Jo, M.S. Lee, and M.B. Ko, *Effects of comonomers and shear on the melt intercalation of styrenics/clay nanocomposites*, Polymer 42 (1) (2001), pp. 329–336. doi:10.1016/S0032-3861(00)00333-5.

[6] S.W. Kim, W.H. Jo, M.S. Lee, M.B. Ko, and J.Y. Jho, *Effects of shear on melt exfoliation of clay in preparation of nylon 6/organoclay nanocomposites*, Polym. J. 34 (3) (2002), pp. 103–111. doi:10.1295/polymj.34.103.

[7] D. Homminga, B. Goderis, S. Hoffman, H. Reynaers, and G. Groeninckx, *Influence of shear flow on the preparation of polymer layered silicate nanocomposites*, Polymer 46 (23) (2005), pp. 9941–9954. doi:10.1016/j.polymer.2005.07.059.

[8] M. Bousmina, *Study of intercalation and exfoliation processes in polymer nanocomposites*, Macromolecules 39 (12) (2006), pp. 4259–4263. doi:10.1021/ma052647f.

[9] M. Alexandre and P. Dubois, *Polymer-layered silicate nanocomposites: Preparation, properties and uses of a new class of materials*, Mater. Sci. Eng. Reports 28 (1–2) (2000), pp. 1–63.

[10] S.S. Ray and M. Okamoto, *Polymer/layered silicate nanocomposites: A review from preparation to processing*, Prog. Polym. Sci. 28 (11) (2003), pp. 1539–1641. doi:10.1016/j.progpolymsci.2003.08.002.

[11] S. Pavlidou and C.D. Papaspyrides, *A review on polymer-layered silicate nanocomposites*, Prog. Polym. Sci. 33 (12) (2008), pp. 1119–1198. doi:10.1016/j.progpolymsci.2008.07.008.

[12] S. Filippi and P. Magagnini, *Polyolefin nanocomposites by solution blending method*, in *Advances in Polyolefin Nanocomposites*, V. Mittal, ed., Taylor & Francis, Boca Raton, FL, 2011.

[13] E. Passaglia and S. Coiai, *Functional polyolefins for polyolefin/clay nanocomposites*, in *Advances in Polyolefin Nanocomposites*, V. Mittal, ed., Taylor & Francis, Boca Raton, FL, 2011.

[14] K. Chrissopoulou and S.H. Anastasiadis, *Polyolefin/layered silicate nanocomposites with functional compatibilizers*, Eur. Polym. J. 47 (4) (2011), pp. 600–613. doi:10.1016/j.eurpolymj.2010.09.028.

[15] S. Filippi, E. Mameli, C. Marazzato, and P. Magagnini, *Comparison of solution-blending and melt-intercalation for the preparation of poly(ethylene-co-acrylic acid)/organoclay nanocomposites*, Eur. Polym. J. 43 (5) (2007), pp. 1645–1659. doi:10.1016/j.eurpolymj.2007.02.015.

[16] S. Filippi, C. Marazzato, P. Magagnini, A. Famulari, P. Arosio, and S.V. Meille, *Structure and morphology of HDPE-g-MA/organoclay nanocomposites: Effects of the preparation procedures*, Eur. Polym. J. 44 (4) (2008), pp. 987–1002. doi:10.1016/j.eurpolymj.2008.01.011.

[17] Q. Zhang, X. Ma, Y. Wang, and K. Kou, *Morphology and interfacial action of nanocomposites formed from ethylene−vinyl acetate copolymers and organoclays*, J. Phys. Chem. B. 113 (35) (2009), pp. 11898–11905. doi:10.1021/jp903448t.

[18] L. Cui, X. Ma, and D.R. Paul, *Morphology and properties of nanocomposites formed from ethylene–vinyl acetate copolymers and organoclays*, Polymer 48 (21) (2007), pp. 6325–6339. doi:10.1016/j.polymer.2007.08.040.

[19] K.M. Lee and C.D. Han, *Rheology of organoclay nanocomposites: Effects of polymer matrix/organoclay compatibility and the gallery distance of organoclay*, Macromolecules 36 (19) (2003), pp. 7165–7178. doi:10.1021/ma030302w.

[20] X. Li and C.S. Ha, *Nanostructure of EVA/organoclay nanocomposites: Effects of kinds of organoclays and grafting of maleic anhydride onto EVA*, J. Appl. Polym. Sci. 87 (12) (2003), pp. 1901–1909. doi:10.1002/app.11922.

[21] D.S. Chaudhary, R. Prasad, R.K. Gupta, and S.N. Bhattacharya, *Clay intercalation and influence on crystallinity of EVA-based clay nanocomposites*, Thermochim. Acta 433 (1–2) (2005), pp. 187–195.
[22] S. Peeterbroeck, M. Alexandre, and R. Jérôme, P.H. Dubois, *Poly(ethylene-co-vinyl acetate)/clay nanocomposites: Effect of clay nature and organic modifiers on morphology, mechanical and thermal properties*, Polym. Degrad. Stab. 90 (2) (2005), pp. 288–294. doi:10.1016/j.polymdegradstab.2005.03.023.
[23] C.G. Martins, N.M. Larocca, D.R. Paul, and L.A. Pessan, *Nanocomposites formed from polypropylene/EVA blends*, Polymer 50 (7) (2009), pp. 1743–1754. doi:10.1016/j.polymer.2009.01.059.
[24] S. Filippi, M. Paci, F. Baldanzi, D. Rossi, and G. Polacco, *XRD study of intercalation in statically annealed composites of ethylene copolymers and organically modified montmorillonites. 1. Two-tailed organoclays*, J. Taiwan Inst. Chem. Eng. 44 (2013), pp. 123–130. doi:10.1016/j.jtice.2012.09.002.
[25] Y. Tian, H. Yu, S. Wu, G. Ji, and J. Shen, *Study on the structure and properties of EVA/clay nanocomposites*, J. Mater. Sci. 39 (13) (2004), pp. 4301–4303. doi:10.1023/B:JMSC.0000033412.92494.ee.
[26] M. Zanetti, G. Camino, R. Thomann, and R. Mülhaupt, *Synthesis and thermal behaviour of layered silicate–EVA nanocomposites*, Polymer 42 (10) (2001), pp. 4501–4507. doi:10.1016/S0032-3861(00)00775-8.
[27] J.E.F.C. Gardolinski and G. Lagaly, *Grafted organic derivatives of kaolinite: II. Intercalation of primary n-alkylamines and delamination*, Clay Miner. 40 (4) (2005), pp. 547–556. doi:10.1180/0009855054040191.
[28] W. Zhang, D. Chen, Q. Zhao, and Y.Y. Fang, *Effects of different kinds of clay and different vinyl acetate content on the morphology and properties of EVA/clay nanocomposites*, Polymer 44 (26) (2003), pp. 7953–7961. doi:10.1016/j.polymer.2003.10.046.
[29] F. Cser and S.N. Bhattacharya, *Study of the orientation and the degree of exfoliation of nanoparticles in poly(ethylene–vinyl acetate) nanocomposites*, J. Appl. Polym. Sci. 90 (11) (2003), pp. 3026–3031. doi:10.1002/app.13026.
[30] M. Zanetti, T. Kashiwagi, L. Falqui, and G. Camino, *Cone calorimeter combustion and gasification studies of polymer layered silicate nanocomposites*, Chem. Mater. 14 (2) (2002), pp. 881–887. doi:10.1021/cm011236k.
[31] C.H. Jeon, S.H. Ryu, and Y.W. Chang, *Preparation and characterization of ethylene vinyl acetate copolymer/montmorillonite nanocomposite*, Polym. Int. 52 (2003), pp. 153–157. doi:10.1002/pi.1066.
[32] S. Duquesne, C. Jama, M. Le Bras, R. Delobel, P. Recourt, and J.M. Gloaguen, *Elaboration of EVA–nanoclay systems – characterization, thermal behaviour and fire performance*, Comp. Sci. Technol. 63 (2003), pp. 1141–1148. doi:10.1016/S0266-3538(03)00035-6.
[33] M.C. Costache, D.D. Jiang, and C.A. Wilkie, *Thermal degradation of ethylene–vinyl acetate coplymer nanocomposites*, Polymer 46 (2005), pp. 6947–6958. doi:10.1016/j.polymer.2005.05.084.
[34] K.-N. Kim, H. Kim, and J.-W. Lee, *Effect of interlayer structure, matrix viscosity and composition of a functionaiized polymer on the phase structure of polypropylene–montmorillonite nanocomposites*, Polym. Eng. Sci. 41 (2001), pp. 1963–1969. doi:10.1002/pen.10892.
[35] C.I. Park, M.H. Kim, and O.O. Park, *Effect of heat treatment on the microstructural change of syndiotactic polystyrene/poly(styrene-co-vinyloxazolin)/clay nanocomposite*, Polymer 45 (2004), pp. 1267–1273. doi:10.1016/j.polymer.2003.12.011.
[36] B.N. Jang, D. Wang, and C.A. Wilkie, *Relationship between the solubility parameter of polymers and the clay dispersion in polymer/clay nanocomposites and the role of the surfactant*, Macromolecules 38 (2005), pp. 6533–6543. doi:10.1021/ma0508909.
[37] F. Perrin-Sarazin, M.-T. Ton-That, M.N. Bureau, and J. Denault, *Micro- and nano-structure in polypropylene/clay nanocomposites*, Polymer 46 (2005), pp. 11624–11634. doi:10.1016/j.polymer.2005.09.076.
[38] C.O. Rohlmann, M.F. Horst, L.M. Quinzani, and M.D. Failla, *Comparative analysis of nanocomposites based on polypropylene and different montmorillonites*, Eur. Polym. J. 44 (2008), pp. 2749–2760. doi:10.1016/j.eurpolymj.2008.07.006.

[39] S. Benali, S. Peeterbroeck, J. Larrieu, F. Laffineur, J.-J. Pireaux, M. Alexandre, and P. Dubois, *Study of interlayer spacing collapse during polymer/clay nanocomposite melt intercalation*, J. Nanosci. Nanotech. 8 (2008), pp. 1707–1713. doi:10.1166/jnn.2008.020.
[40] T.D. Fornes, P.J. Yoon, and D.R. Paul, *Polymer matrix degradation and color formation in melt-processed nylon 6/clay nanocomposites*, Polymer 44 (2003), pp. 7545–7556. doi:10.1016/j.polymer.2003.09.034.
[41] G. Edwards, P. Halley, G. Kerven, and D. Martin, *Thermal stability analysis of organo-silicates, using solid phase microextraction techniques*, Thermochim. Acta 429 (2005), pp. 13–18. doi:10.1016/j.tca.2004.11.020.
[42] A. Montagnani, *Preparazione e caratterizzazione morfologica di nanocompositi a base di polietileni funzionalizzati*, Thesis, University of Pisa, 2010.